ASME J. HEAT AND MASS TRANSFER

https://asmedigitalcollection.asme.org/heattransfer

ACCEPTED DECEMBER 19TH 2024

THERMO-MAGNETIC BIOCONVECTION FLOW IN A SEMI-TRAPEZOIDAL ENCLOSURE FILLED WITH A POROUS MEDIUM CONTAINING OXYTACTIC MICRO-ORGANISMS: *MODELLING HYBRID MAGNETIC BIO-FUEL CELLS*

K. Venkatadri[1], P. Rajarajeswari[2*], O. Anwar Bég[3], V. Ramachandra Prasad[4], H.J. Leonard[3] and S. Kuharat[3]

[1]Department of Mathematics, Mohan Babu University (Erstwhile Sree Vidyanikethan Engineering college), Tirupati, A.P., 517102, India. Email: venkatadri.venki@gmail.com , venkatadri.k@mbu.asia

[2]Department of Software systems, School of Computer Science and Engineering, Vellore Institute of Technology, Vellore -632014, Tamilnadu, **India**.*

*[3]MPESG, Corrosion Lab, 3-08, Aeronautical and Mechanical Engineering Division, SEE Building, University of Salford, M5 4WT, **England, UK**. Emails: O.A.Beg@salford.ac.uk; H.Leonard@salford.ac.uk S.Kuharat2@salford.ac.uk*

*[4]Department of Mathematics, School of Advanced Sciences, Vellore Institute of Technology, Vellore – 632014, **India**. Email: rcpmaths@gmail.com*

****Corresponding Author: rajacse77@gmail.com***

ABSTRACT:

Hybrid fuel cells are becoming increasingly popular in 21st century energy systems engineering. These systems combine multiple features including various geometries, electromagnetic fluids, bacteria (micro-organisms), thermo-solutal convection and porous media. Motivated by these developments in the present work we simulate the two-dimensional magnetohydrodynamic (MHD) natural triple convection flow in a semi-trapezoidal enclosure saturated with electrically conducting water containing oxytactic microorganisms and oxygen species. The Darcy-Brinkman model is deployed for porous media drag effects. The primitive governing partial differential conservation equations for mass, momentum, energy, oxygen species and motile micro-organism species density are transformed using a vorticity-stream function formulation and non-dimensional variables into a nonlinear boundary value problem. A numerical solution is obtained using a finite difference method with incremental time steps. The mathematical model features a number of controlling parameters i.e. Prandtl number, Rayleigh number, Bioconvective Rayleigh number, Darcy parameter, Hartmann (magnetic body force) number, Lewis number, Péclet number, Oxygen diffusion ratio, fraction of consumption oxygen to diffusion of oxygen parameter. Transport characteristics (streamlines, isotherms, oxygen iso-concentration and motile micro-organism concentration) are computed for several of these parameters. Microorganisms' impact on the rate of heat transfer at the boundaries is found to be beneficial or destructive, depending on combination of other parameters in the simulations. Additionally, Nusselt number and oxygen species Sherwood number are computed at the hot vertical wall. The simulations are relevant to hybrid electromagnetic microbial fuel cells.

KEYWORDS: *Vorticity-stream function, semi-trapezoidal enclosure, hybrid fuel cells; Oxytactic bacteria, bioconvection; magnetohydrodynamics (MHD), porous medium; oxygen consumption.*

1.INTRODUCTION

The capacity of microorganisms to swim under a particular stimulus or taxis is known as bioconvection. It is increasingly being deployed in fuel cell technologies [1, 2]. Many different types of bioconvection arise in nature including photo-taxis, geo-taxis, gyro-taxis and chemotaxis (reflecting the response of microorganisms to light, gravity, torque and chemical concentration) etc. Bioconvection is generally induced by unstable density stratification which is caused by up-swimming microorganisms. This unstable density stratification is produced when the microorganisms, which possess greater density than water, cluster in the upper regions of the fluid. Bioconvection has also been combined with porous media to achieve interesting results of relevance to fuel cells and other industrial technologies. Important studies in this regard include Kessler [3,4] who observed that a porous medium can be deployed to manipulate bioconvection and achieve for example elimination of harmful fungi from cultures. Many complex features can arise in bioconvection flows including plumes, bio-thermal convection etc. Bioconvection offers considerable promise in modern fuel cell technology [5]. It has also been exploited in lubrication engineering and tribological enhancement [6,7]. Two particularly popular bioconvection mechanisms are gyrotactic which are torque-driven and oxytactic which is oxygen-driven. Nima et al. [8] investigated theoretically the free-forced convective gyrotactic bioconvection flow in a Darcian porous medium fuel cell. They applied the finite difference method and also symbolic Maple 14.0 software to simulate the impact of buoyancy and bioconvection parameters on temperature, velocity, oxygen concentration and motile micro-organism density distribution, Nusselt number, Sherwood number and motile microorganism density gradient. They showed that gyrotactic microorganisms can be judiciously deployed to enhance both thermal and momentum transport characteristics in fuel cells. Another important application of bioconvection is microbial fuel cells in which for example, bio-electrochemical process can be exploited to generate electricity by using the electrons derived from biochemical reactions catalysed by motile micro-organisms (bacteria). Microbial fuel cells feature oxidation and may be mediated or unmediated. Oxidation and oxygen fate in such systems is a critical issue [9-11]. Other important potential applications of bioconvection include bacterial oxygen generation [12], water treatment with phototrophic bacteria [13], phytoremediation [14] and water treatment optimization [15, 16].

A new development in bio-fuel cells has been the deployment of magnetic fields. Electromagnetic bio-fuel cells [17, 18] simultaneously deploy magnetohydrodynamics (MHD) and bioconvection mechanisms. Okada et al. [19] have investigated magnetic field gradients on electrochemical oxygen reduction in polymer electrolyte fuel (PEM) cells. They emphasized the influence of magnetic attractive force toward oxygen and noted that fuel cell performance can be enhanced with judicious deployment of magnetic field intensity. Zhou et al. [20] investigated magnetic microbial fuel cells (MFCs) over a range of static magnetic field (SMF) and observed an enhancement in exo-electrogenic biofilm production. Li et al. [21] who studied static magnetic field influence on electricity generation in microbial fuel cells. Further experimental investigations include Tong et al. [22], Yin et al. [23] and Sakai et al. [24] in which magnetic field has been shown to be manipulate biological fuel cell performance. Theoretical and computational studies of magnetohydrodynamic (MHD) bioconvection in enclosures have also been communicated in recent years. Taheri and Bilgen [25] used a control volume numerical method to investigate the gravitactic bioconvection in rectangular enclosures. They computed the effects of a range of bioconvection Péclet numbers on the stability of the flow. They noted critical Rayleigh number is reduced with elevation in bioconvection Péclet number and larger aspect ratio. Hussain et al. [26] used a Galerkin-based finite element method to compute the bioconvection of oxytactic microorganisms in an omega-shaped porous enclosure containing nano-encapsulated phase change materials (NEPCMs). They noted that both oxygen and motile micro-organism iso-concentration is strongly increased with increment in bioconvection Rayleigh number. Balla et al. [27] investigated numerically bioconvection of oxytactic microorganisms in a square enclosure containing porous medium with thermal radiative heat flux. They considered the Darcy model of Boussinesq approximation. They noted that bioconvection patterns are intensified with larger Rayleigh number and suppressed with thermal radiation parameter. They also noted oxygen density and motile iso-concentration are both considerably boosted with Rayleigh number and radiation parameter.

An inspection of the literature has shown that further investigations are warranted regarding the *impact of bioconvection micro-organisms on fuel cell performance in the presence of magnetic fields with oxygen depletion (consumption)*. Micro-organisms in the studies mentioned earlier [24-27] may variously intensify or suppress heat transfer rates depending on magnetic field intensity or other factors including porous media and oxygen levels. A detailed analysis is therefore presented to elucidate in more detail the thermal/species/momentum characteristics in two-dimensional magnetohydrodynamic (MHD) natural triple convection flow in a semi-trapezoidal enclosure saturated with electro-conductive water containing oxytactic microorganisms and oxygen species. Darcy's model is used to simulate porous media drag effects. The transport equations for mass, momentum, energy, oxygen species and motile micro-organism species density are rendered non-dimensional using a vorticity-stream function formulation and non-dimensional variables into a nonlinear boundary value problem. A robust finite difference method [28, 29] with incremental time steps is deployed to obtain computational solutions. Mesh independence and validation with previous studies is included. The transport characteristics (streamlines, isotherms, species iso-concentration and motile micro-organism concentration) are computed for a wide range of involved controlling parameters i.e. Prandtl number, Rayleigh number, Bioconvective Rayleigh number, Darcy parameter, Hartmann (magnetic body force) number, Lewis number, Péclet number, Oxygen diffusion ratio, fraction of consumption oxygen to diffusion of oxygen parameter. It is envisaged that the present simulations will provide further insight into improving performance characteristics of hybrid MHD bioconvection fuel cells [20-23].

2. MATHEMATICAL FORMULATION:

The physical model is illustrated in **Fig. 1** with reference to an (x, y) coordinate system. The regime studied comprises incompressible, laminar unsteady two-dimensional buoyancy driven flow in a semi-trapezium cavity containing a Darcian porous medium saturated with Newtonian electroconductive water and containing oxygen species and self-propelling motile micro-organisms. A temperature T_h is prescribed along the right vertical hot wall (height H) and T_c at the cold inclined left wall. The upper wall (length *2H*) and lower horizontal wall (length *H*) are adiabatic. All boundaries are electrically insulated, and the no slip velocity condition is imposed on the interior surfaces. We examine triple convective phenomena (heat, oxygen species and bacterial micro-organisms). The enclosure (fuel cell) is subjected to a horizontal static magnetic field, with intensity, B_o in the enclosure which generates a Lorentz force due to the mutual interaction of the imposed magnetic field and fuel cell fluid through its electrical conducting characteristics and $\mathbf{j} = \sigma\left(\mathbf{E} + \mathbf{V} \times \mathbf{B}\right)$ with a zero electric field intensity, $\mathbf{E} = 0$. This magnetic body force acts in the vertical downward direction. Magnetic induction effects are neglected as the magnetic Reynolds number is sufficiently low in magnitude.

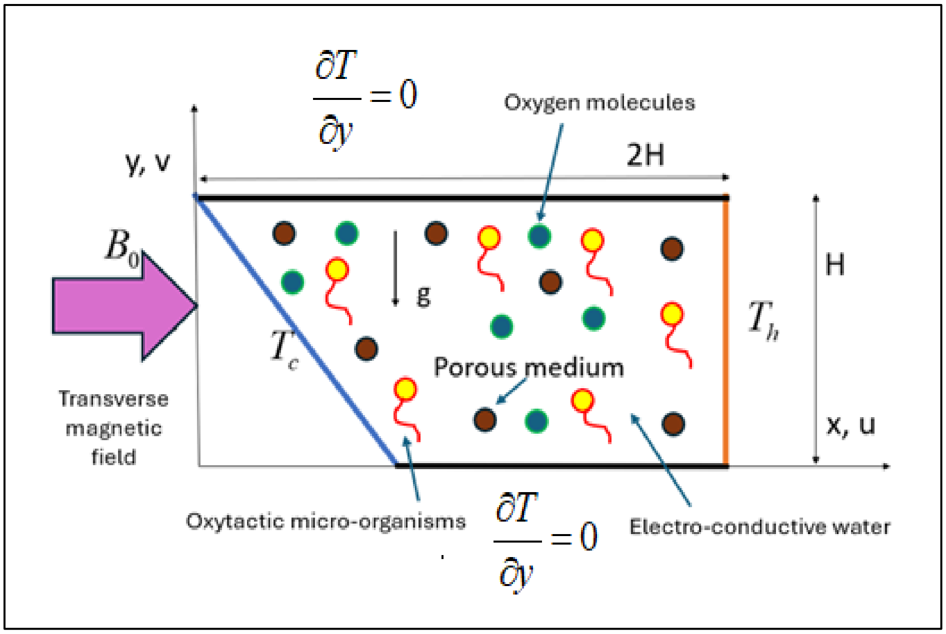

Fig 1: Physical model for hybrid porous medium magnetic bioconvection fuel cell

Electrical polarization and Hall current effects are ignored as are viscous dissipation, thermal dispersion and thermal stratification. The micro-organisms are assumed to be much smaller than the pore dimensions and the percolating water and porous medium are in local thermal equilibrium. Darcian drag forces appear in both the x- and y-momentum conservation equations. Thermal buoyancy and species buoyancy force are also present. Under these assumptions, and utilizing the Boussinesq approximation for buoyancy, following Hussain and Geridonmez [30], the governing equations can be presented as follows:

$$\frac{\partial u}{\partial x}+\frac{\partial v}{\partial y}=0 \tag{1}$$

$$\frac{\partial u}{\partial t}+u\frac{\partial u}{\partial x}+v\frac{\partial u}{\partial y}=-\frac{1}{\rho}\frac{\partial p}{\partial x}+\nu\left[\frac{\partial^2 u}{\partial x^2}+\frac{\partial^2 u}{\partial y^2}\right]-\frac{\nu}{K}u \tag{2}$$

$$\frac{\partial v}{\partial t}+u\frac{\partial v}{\partial x}+v\frac{\partial v}{\partial y}=-\frac{1}{\rho}\frac{\partial p}{\partial y}+\nu\left[\frac{\partial^2 v}{\partial x^2}+v\frac{\partial^2 v}{\partial y^2}\right]-\frac{\nu}{K}v-\frac{\sigma}{\rho}B_o^2 v-\frac{1}{\rho}\left[\gamma\Delta\rho.n-\rho\beta_T(T-T_c)\right]g \tag{3}$$

$$\frac{\partial T}{\partial t}+u\frac{\partial T}{\partial x}+v\frac{\partial T}{\partial y}=\alpha\left[\frac{\partial^2 T}{\partial x^2}+v\frac{\partial^2 T}{\partial y^2}\right] \tag{4}$$

$$\frac{\partial C}{\partial t}+u\frac{\partial C}{\partial x}+v\frac{\partial C}{\partial y}=D_c\left[\frac{\partial^2 C}{\partial x^2}+v\frac{\partial^2 C}{\partial y^2}\right]-\lambda n \tag{5}$$

$$\frac{\partial n}{\partial t}+\frac{\partial}{\partial x}\left[un+\bar{u}n-D_n\frac{\partial n}{\partial x}\right]+\frac{\partial}{\partial y}\left[vn+\bar{v}n-D_n\frac{\partial n}{\partial y}\right]=0 \tag{6}$$

Here *(u,v) are the (x,y) velocity components, t is time, ρ is water density, p is pressure,* ν *is kinematic viscosity of water, K is porous medium permeability,* σ *is electrical conductivity,* B_o *is static magnetic field strength,* $\tilde{u}=\frac{bWc}{\Delta C}\frac{\partial C}{\partial x}$ *and* $\tilde{v}=\frac{bWc}{\Delta C}\frac{\partial C}{\partial y}$ *are mean swimming velocities of the micro-organisms in the x, y directions, b is a bioconvection constant,* W_c *denotes maximum swimming speed,* $\Delta C = C_o - C_{min}$ *where* C_o *denotes the oxygen concentration at the left wall and* C_o *is the minimum oxygen concentration at the right hot wall,* γ *is the mean volume of bacteria (micro-organisms), n denotes motile micro-organism density number, g is gravity,* β_T *is thermal expansion coefficient, T is temperature of fluid (water),* α *is thermal diffusivity, C is oxygen species concentration,* λ *is oxygen consumption rate,* D_c *is oxygen molecular diffusivity and* D_n *is the micro-organism (bacterial) diffusivity*. The primitive equations (1)- (6) can be simplified by introducing scaling transformations which are defined as follows:

$$\tau=\frac{t\alpha}{H^2};X=\frac{x}{H};Y=\frac{y}{H};U=\frac{uH}{\alpha};V=\frac{vH}{\alpha};\theta=\frac{T-T_c}{T_h-T_c};P=\frac{pL^2}{\rho\alpha^2};$$
$$\varphi=\frac{C-C_{\min}}{\Delta C};N=\frac{n}{n_o};\ \psi=\frac{\bar{\psi}}{\alpha};\ \omega=\frac{\bar{\omega}H^2}{\alpha} \tag{7}$$

Here τ *is dimensionless time variable, (X, Y) are dimensionless (x, y) coordinates, U, V are dimensionless (X, Y) velocity components,* θ *is non-dimensional temperature function, P is dimensionless pressure,* φ *is dimensionless oxygen concentration, N is dimensionless motile micro-organism density number,* ψ *is dimensionless stream function,* ω *is dimensionless vorticity,* $\tilde{\psi}$ *is dimensional stream function and* $\tilde{\omega}$ *is dimensional vorticity*. Introducing a vorticity-stream function (ω-ψ) formulation, we define:

$$\frac{\partial^2\psi}{\partial X^2}+\frac{\partial^2\psi}{\partial Y^2}=-\omega \tag{8}$$

$$U = \frac{\partial \psi}{\partial Y} \ and \ \ V = -\frac{\partial \psi}{\partial X} \tag{9}$$

By virtue of Eqns. (7)-(9), the conservation equations (1)-(6) assume the following non-dimensional form:

$$\frac{\partial \omega}{\partial \tau} + U\frac{\partial \omega}{\partial X} + V\frac{\partial \omega}{\partial Y} = \Pr\left[\frac{\partial^2 \omega}{\partial X^2} + \frac{\partial^2 \omega}{\partial Y^2}\right] - \frac{\Pr}{Da}\omega - Ha^2 \Pr\frac{\partial V}{\partial X} + Ra\Pr\left[\frac{\partial \theta}{\partial X} - Rb\frac{\partial N}{\partial X}\right] \tag{10}$$

$$\frac{\partial \theta}{\partial \tau} + U\frac{\partial \theta}{\partial X} + V\frac{\partial \theta}{\partial Y} = \left[\frac{\partial^2 \theta}{\partial X^2} + \frac{\partial^2 \theta}{\partial Y^2}\right] \tag{11}$$

$$\frac{\partial \phi}{\partial \tau} + U\frac{\partial \phi}{\partial X} + V\frac{\partial \phi}{\partial Y} = \frac{1}{Le}\left[\frac{\partial^2 \phi}{\partial X^2} + \frac{\partial^2 \phi}{\partial Y^2}\right] - \frac{\sigma_1}{Le}N \tag{12}$$

$$\begin{aligned}\chi\left[\frac{\partial N}{\partial \tau} + U\frac{\partial N}{\partial x} + V\frac{\partial N}{\partial y}\right] &= \frac{1}{Le}\left[\frac{\partial^2 N}{\partial x^2} + \frac{\partial^2 N}{\partial y^2}\right] \\ &- \frac{Pe}{Le}\left[N\frac{\partial^2 \varphi}{\partial x^2} + N\frac{\partial^2 \phi}{\partial y^2} + \frac{\partial N}{\partial x}\frac{\partial \phi}{\partial x} + \frac{\partial N}{\partial y}\frac{\partial \phi}{\partial y}\right]\end{aligned} \tag{13}$$

The following non-dimensional boundary conditions are imposed at the walls of the fuel cell enclosure:

$$\begin{aligned}&\psi = 0\ ,\ \theta = 0,\ \ \phi = 1,\ \ N = 1,\ \ at\ X + Y = 1\\ &\psi = 0\ ,\ \theta = 1,\ \ \phi = 1,\ \ N = 1,\ \ at\ X = 2\\ &\psi = 0\ \ \frac{\partial \theta}{\partial Y} = 0,\ \ \phi = 1,\ \ PeN\frac{\partial \phi}{\partial Y} - \frac{\partial N}{\partial Y} = 0,\ \ at\ Y = 0\\ &\psi = 0\ \ \frac{\partial \theta}{\partial Y} = 0,\ \ \frac{\partial \phi}{\partial Y} = 0,\ \ \frac{\partial N}{\partial Y} = 0,\ \ at\ Y = 1\end{aligned} \tag{14}$$

We further note that homogeneous Dirichlet boundary conditions, $\psi = 0$, are applied on the stream function, ψ, which represents the no-penetration or kinematic boundary condition at the impermeable walls. The no-slip boundary conditions at the solid walls, is $\frac{\partial \psi}{\partial n} = \mathbf{n} \cdot \nabla\psi = 0$.

In Eqns. (1) – (14) the dimensionless numbers which arise are defined in **Table 1**.

Table 1: Dimensionless numbers in model

Prandtl number	$\mathrm{Pr} = \frac{\upsilon}{\alpha}$
Rayleigh number	$\mathrm{Ra} = \frac{g\beta(T_h - T_c)H^3}{\alpha\upsilon}$
Bioconvective Rayleigh number	$\mathrm{Rb} = \frac{g\gamma\Delta\rho n_0 H^3}{\alpha^2\rho}$
Darcy Parameter	$\mathrm{Da} = \frac{K}{H^2}$
Hartmann number	$\mathrm{Ha} = B_0 H\sqrt{\frac{\alpha}{\mu}}$
Lewis number	$Le = \frac{\alpha}{D_C}$
Péclet number	$Pe = \frac{bW_C}{D_n}$
Oxygen diffusion ratio	$\chi = \frac{D_c}{D_n}$
Parameter defining fraction of oxygen consumption to oxygen diffusion.	$\sigma_1 = \frac{n_0\lambda H^2}{D_C\Delta C}$

Important wall characteristics for fuel cell design are the local Nusselt number Nu and oxygen species Sherwood number (Sh) along the right vertical heated wall. These take the following expressions:

$$\mathrm{Nu} = -\left(\frac{\partial\theta}{\partial Y}\right)_{\mathrm{at}X=2} \tag{15}$$

$$\mathrm{Sh} = -\left(\frac{\partial\phi}{\partial Y}\right)_{\mathrm{at}X=2} \tag{16}$$

3. NUMERICAL SOLUTION AND VALIDATION

The transformed non-linear boundary value problem defined by Eqns. (10) – (13) under boundary conditions (14) has been solved by the help of vorticity-stream function formulation and the finite difference method. This involves discretizing the semi-trapezoidal enclosure on a grid to for vorticity, stream function, temperature, and concentration fields. The energy transport equation, oxygen species transport equation and motile micro-organism density number equation, are solved using explicit time-stepping and central difference spatial discretization. The vorticity transport equation, which describes the evolution of vorticity, is solved explicitly using central differences for spatial derivatives and an explicit Euler method for time stepping. The stream function is obtained by solving the Poisson equation iteratively using, for example, Jacobi or Gauss-Seidel iteration. The velocity components are then derived from the stream function. Boundary conditions for velocity, temperature, oxygen concentration and micro-organism density are applied to ensure physical accuracy. The coupled problem is iteratively solved for the velocity components derived from the stream function, and thereafter temperature and oxygen concentration and motile micro-organism density fields are computed. First, we present the average Nusselt numbers of the hot wall of the enclosure with Ra = 10^5, Pr = 6.2, Ha = 0, and absence of Darcy number Da, for different grid sizes (**Table. 2**). The average Nusselt number values are observed with grids of sizes 80 × 40, 100 × 50, 120 × 60, 140×70, 160×80 and 180×90. Therefore, grids of sizes 140 × 70 are considered for the other computational results presented. The current numerical methodology has been deployed in a wide array of fuel cell enclosure thermal fluid dynamics problems and readers are referred to Venkatadri et al. [31-34]. To validate the present numerical code, we have compared streamline and isotherm contours with the earlier study of Venkatadri et al. [35] for the special case of Ra = 10^5, Da = 0.01 with zero nanoparticle volume fraction ($\Phi = 0$ is set in [35] to obtain a comparison, since nanofluids were considered in [35]) and neglecting oxygen and micro-organism concentration equations. Very close correlation has been achieved confirming the accuracy of the present simulations.

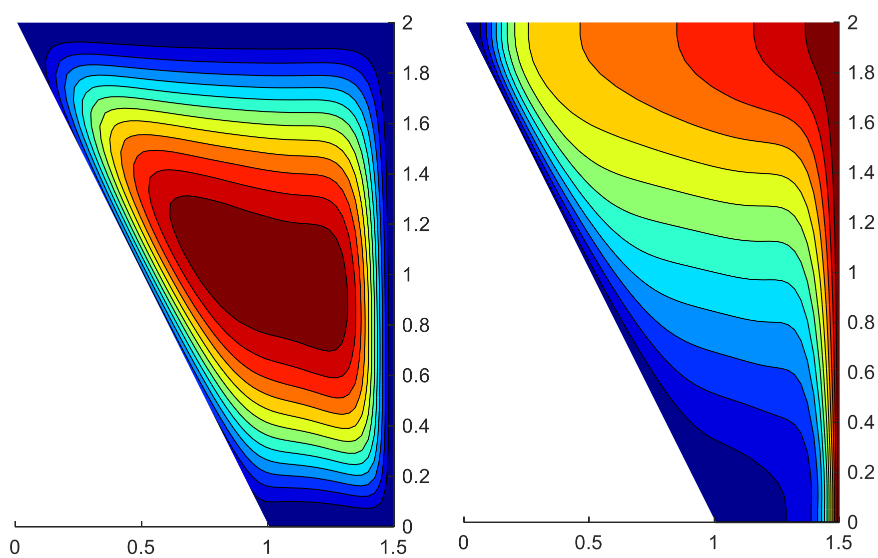

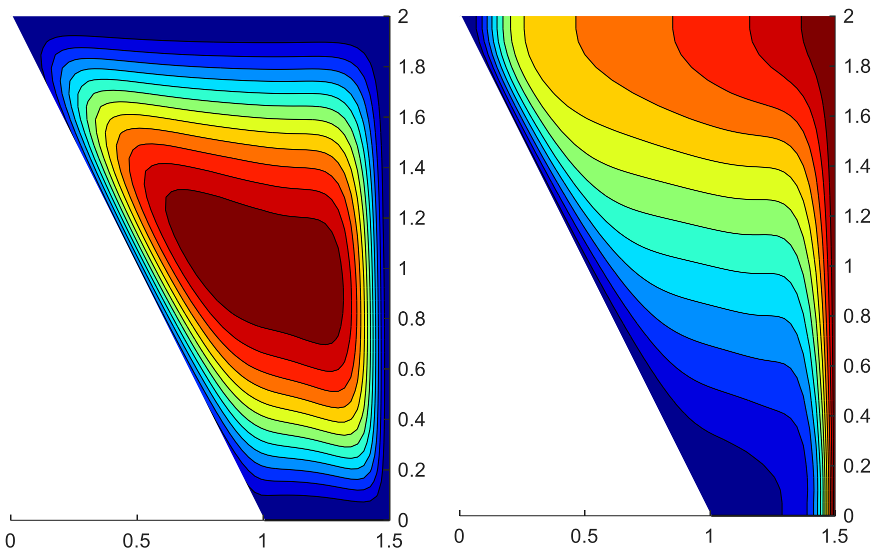

Figure. 2. Comparison of streamline and isotherm contours for Ra = 10^5, Da = 0.01: Top row- numerical results from [35]; Bottom row- present finite difference method computations

Table 2. Grid sensitivity test with Ra = 10^5, Pr = 6.2, Ha = 0, and absence of Darcy number (Da).

Grid size	80 X 40	100 X 50	120 X 60	140 X 70	160 X 80	140 X 140
Nu_{avg}	2.1637	2.2120	2.2641	2.2635	2.2638	2.2637

4. RESULTS AND DISCUSSION:

Detailed computations have been presented in this section for the influence of Prandtl number, Rayleigh number, Bioconvective Rayleigh number, Darcy parameter, Hartmann (magnetic body force) number, Lewis number, Péclet number, Oxygen diffusion ratio, fraction of consumption oxygen to diffusion of oxygen parameter on streamline, isotherm, oxygen iso-concentration contours and motile micro-organism density (concentration) contours. These are shown in **Figs. 3-6**. Additionally, **Figs. 7 to 9** provide graphical solutions for the variation of local Nusselt number and oxygen concentration Sherwood number at the right hot wall of the enclosure.

	ψ	θ
Da =0.0001	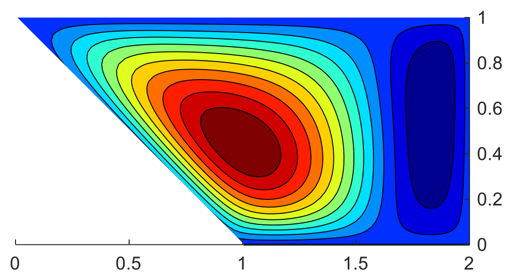	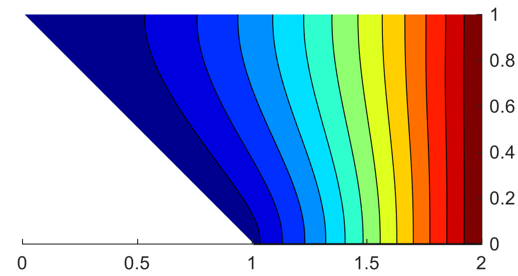
Da = 0.001	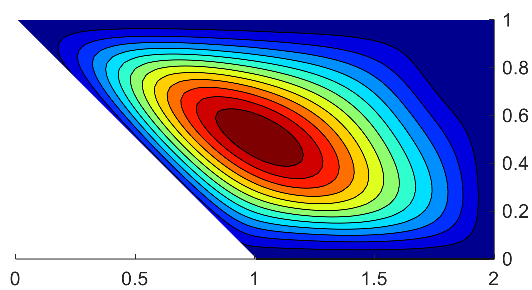	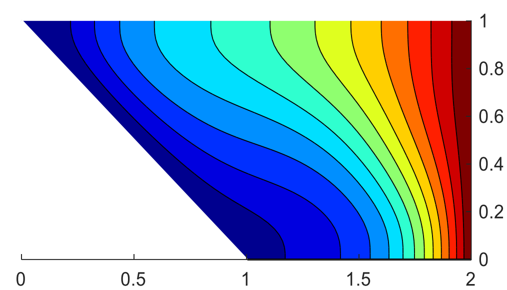
Da = 0.01	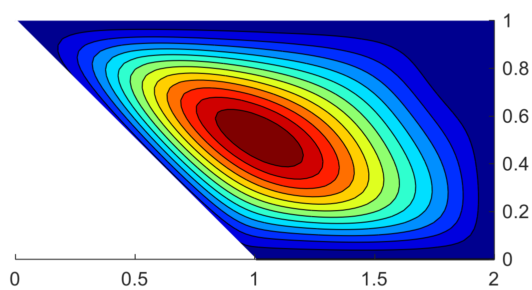	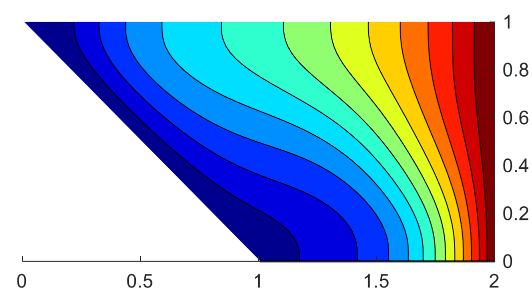

Fig. 3. Streamlines (ψ) and isotherm (θ) contour variation with Darcy number (Da) for Pr = 6.2, Rb = 2.0, Ha = 2, Le = 2, Pe = 1, Ra = 10^5 ,χ =1 and σ_1=1.

	ϕ	N
Da =0.0001	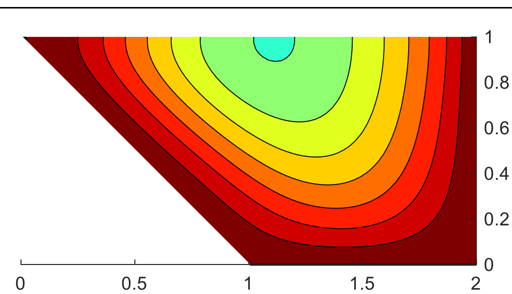	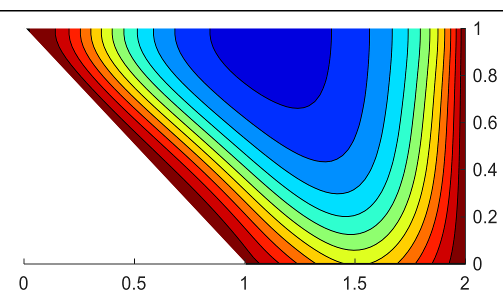

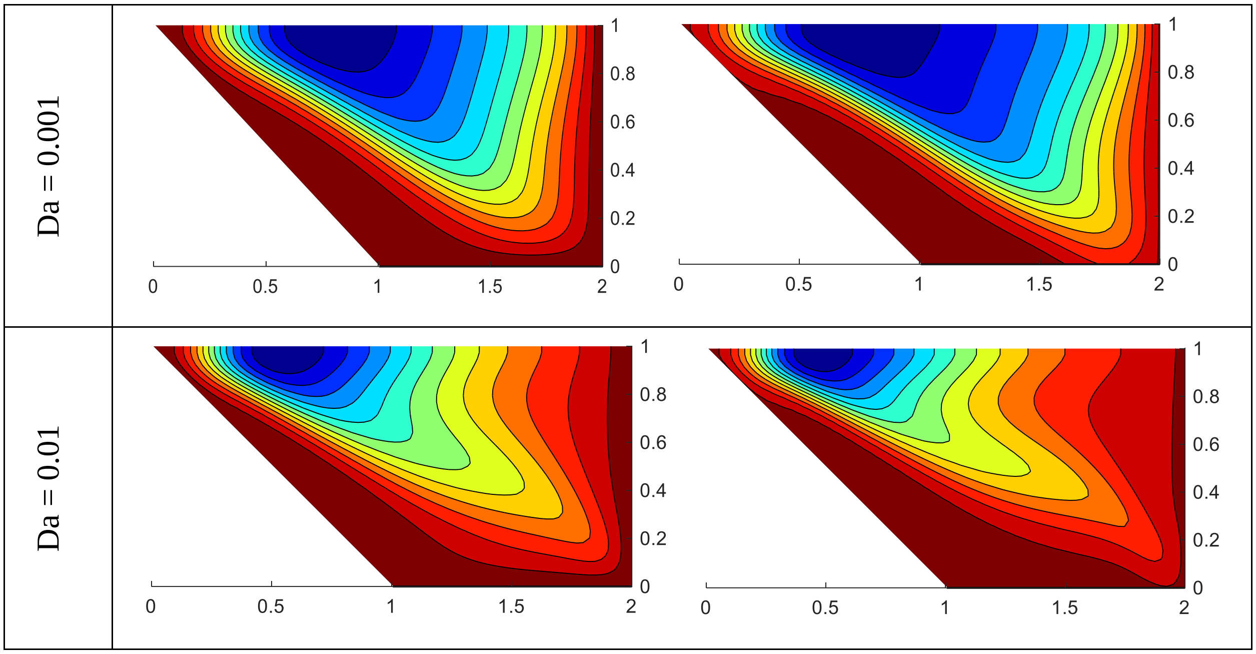

Fig. 4. Oxygen iso-concentration (ϕ) and micro-organism density contours (N) with Darcy number (Da) for $\mathrm{Ra} = 10^5, \chi = 1, \sigma_1 = 1$, Pr = 6.2, Rb = 2.0, Ha = 2, Le = 2, Pe = 1.

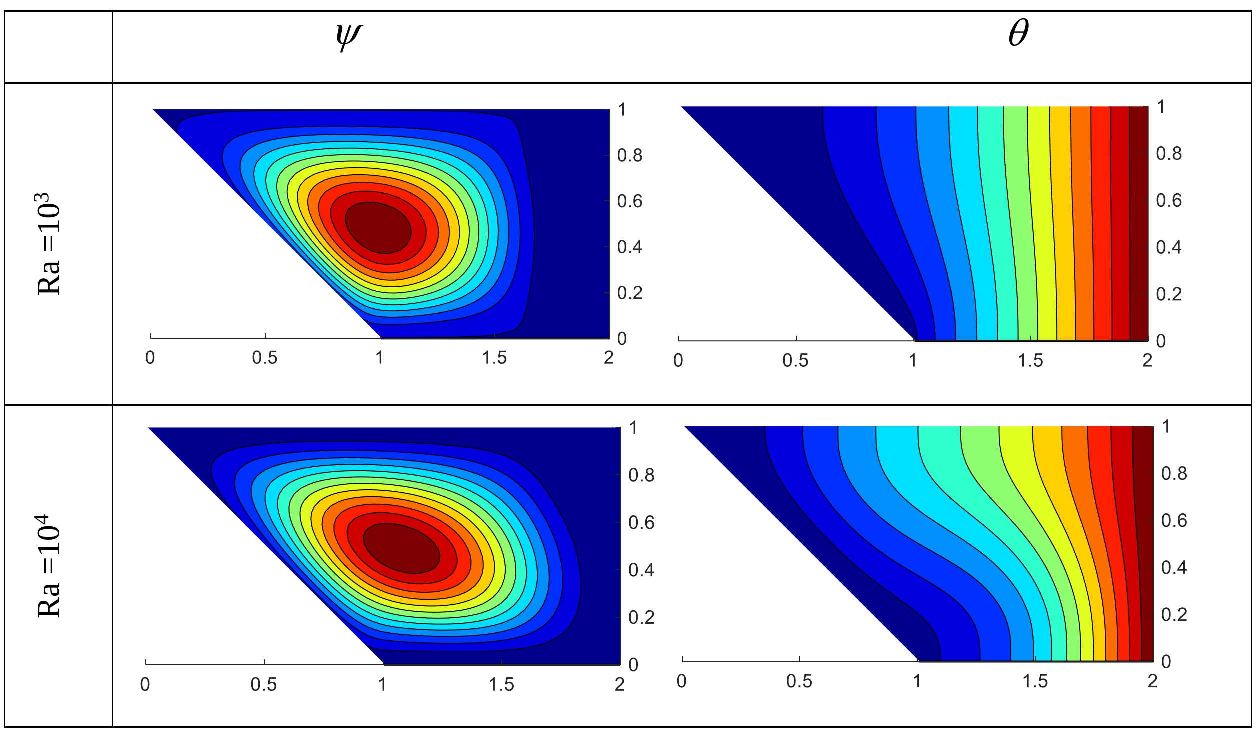

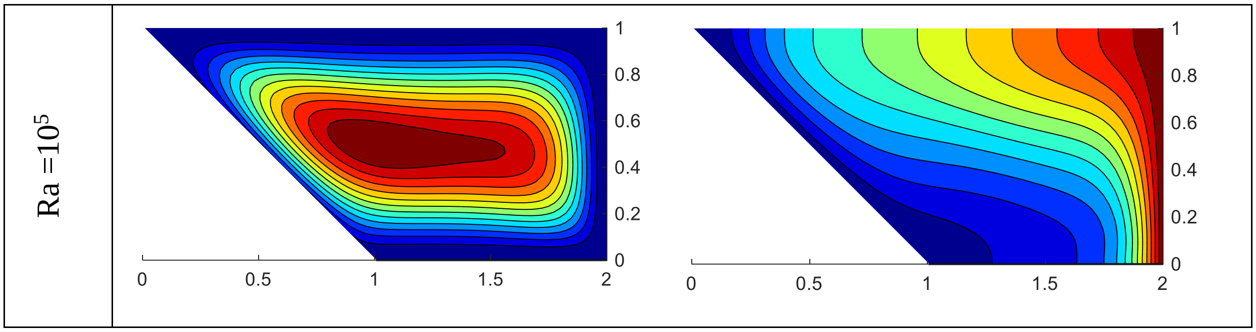

Fig. 5. Streamline (ψ) and isotherm (θ) contours with Ra for Pr = 6.2, Rb = 2.0, Ha = 2, Le = 2, $\mathrm{Pe} = 1, \mathrm{Da} = 0.01, \chi = 1, \sigma_1 = 1$.

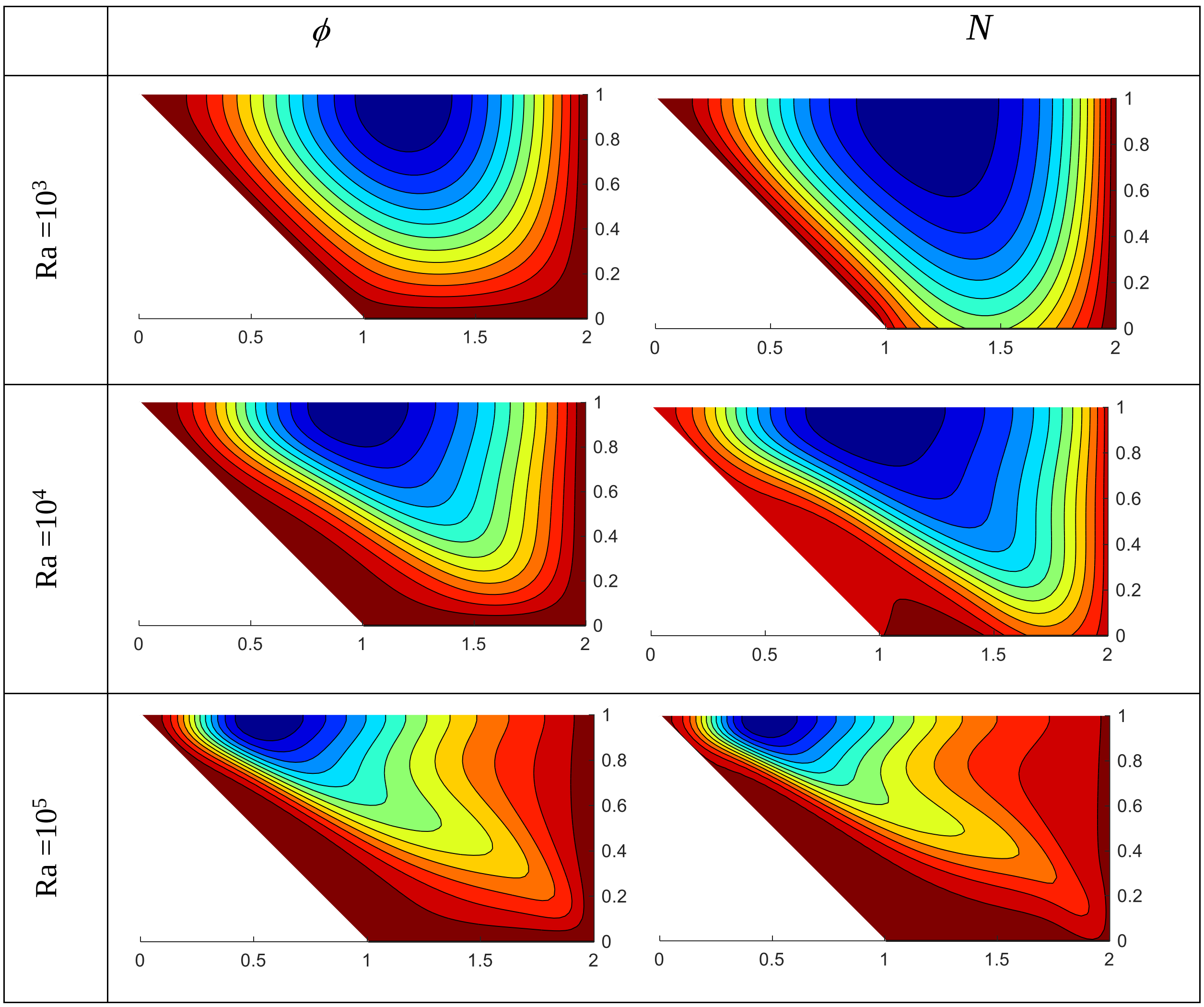

Fig. 6. Oxygen iso-concentration (ϕ) and micro-organism density contours (N) with Ra for $\mathrm{Da} = 0.01, \chi = 1, \sigma_1 = 1$, Pr = 6.2, Rb = 2.0, Ha = 2, Le = 2, Pe = 1.

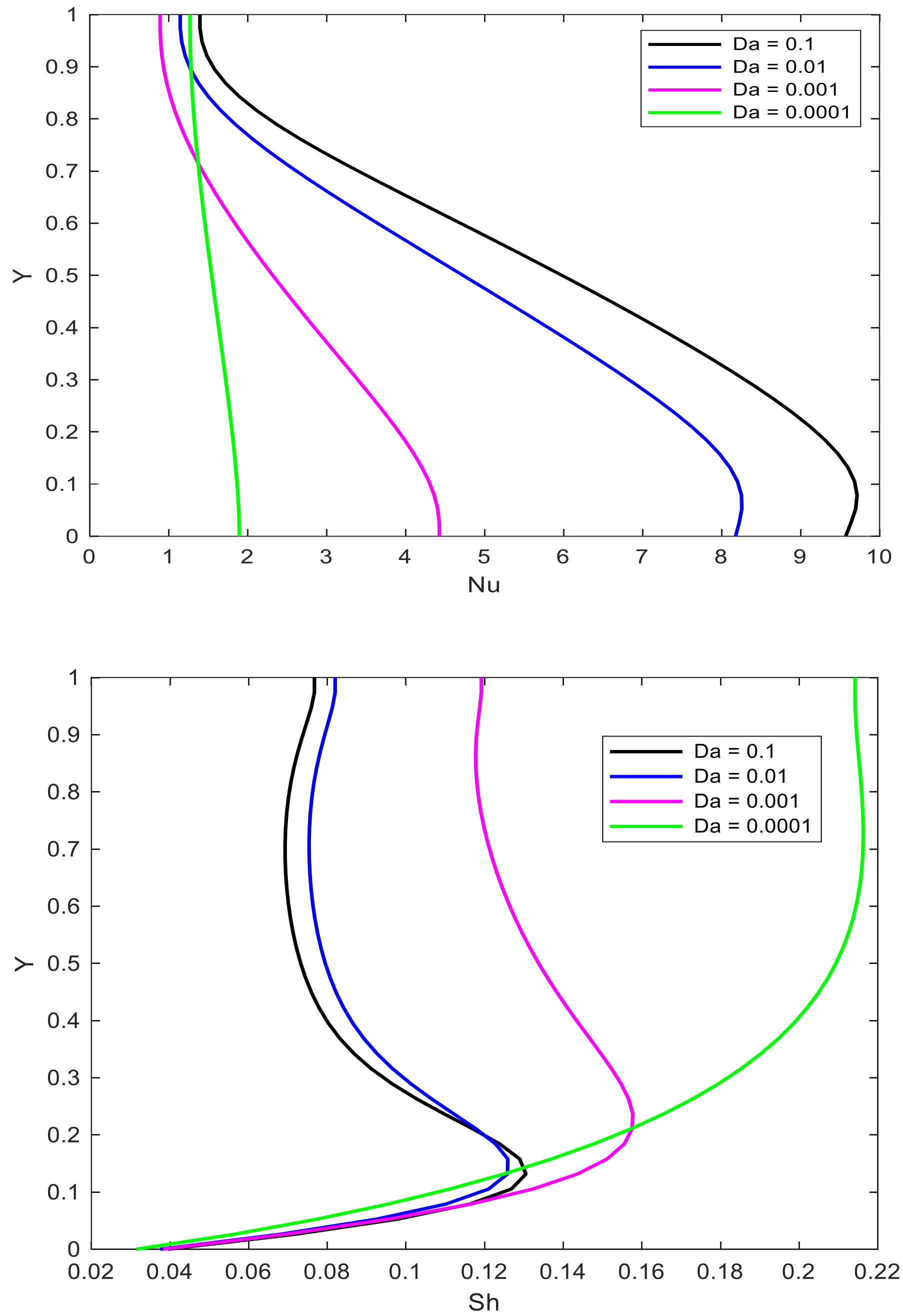

Fig. 7. Local Nusselt number and oxygen species Sherwood number along right wall for various Darcy numbers (Da) with Pr = 6.2, Rb = 2.0, Ha = 2, Le = 2, Pe = 1 $Ra = 10^5, \chi = 1, \sigma_1 = 1$.

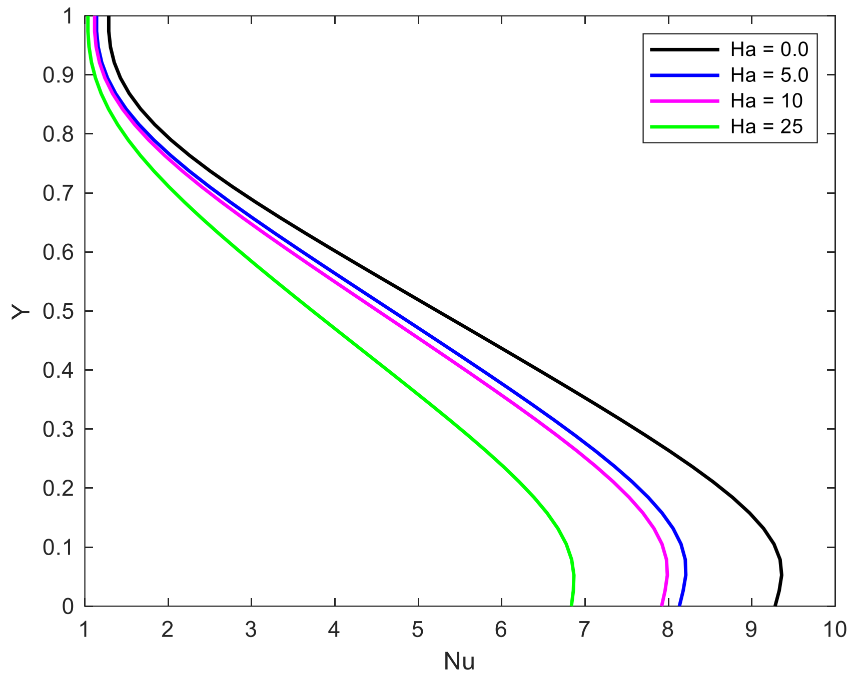

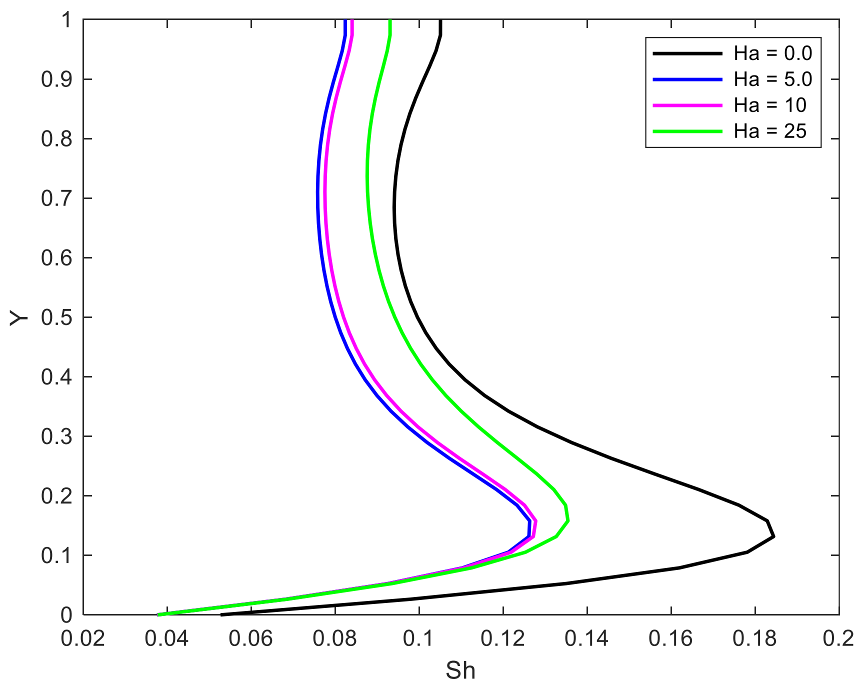

Fig. 8. Local Nusselt number and oxygen species Sherwood number along right wall for various Hartmann numbers (Ha) with Pr = 6.2, Rb = 2.0, Da = 0.01, Le = 2, Pe = 1

$$Ra = 10^5, \chi = 1, \sigma_1 = 1.$$

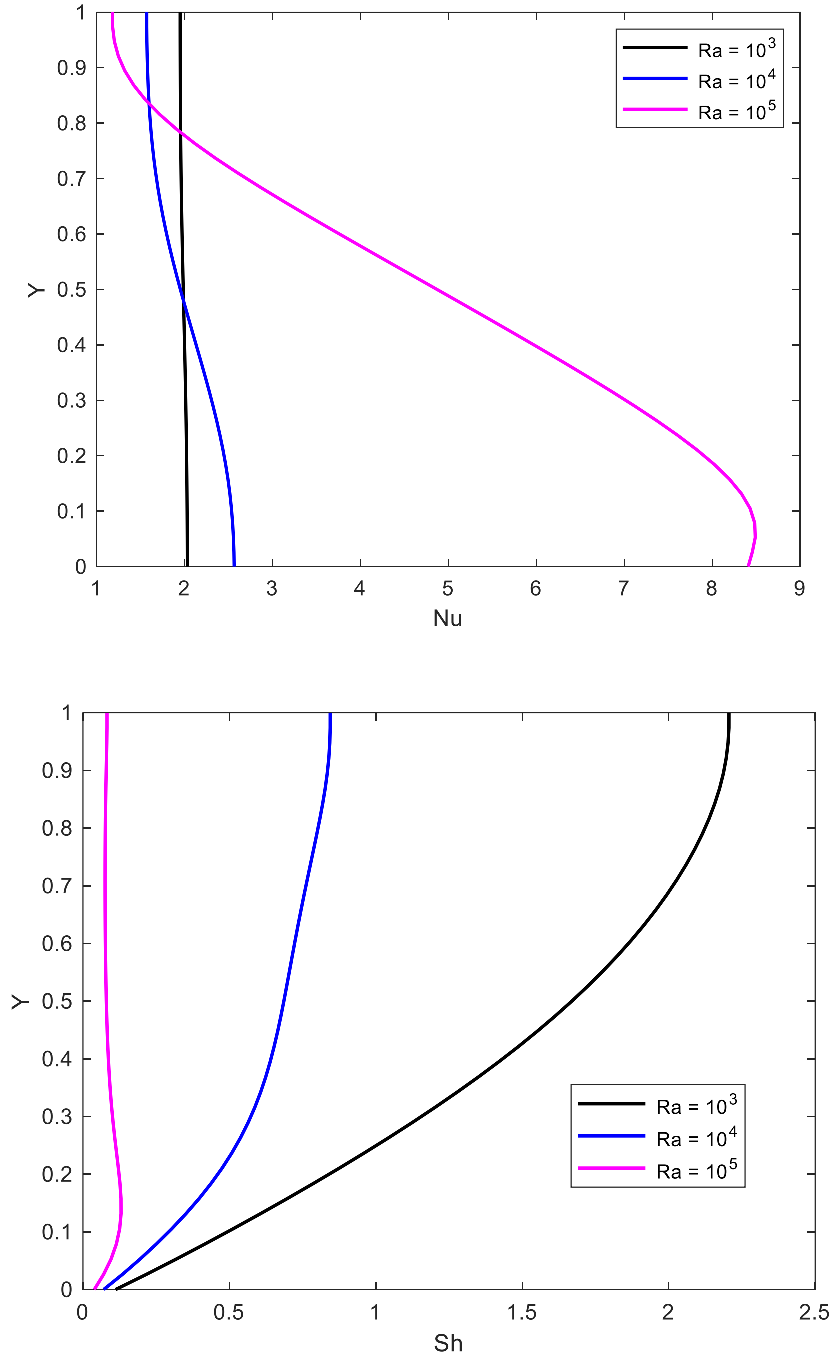

Fig. 9. Local Nusselt number and oxygen species Sherwood number along right wall for various Rayleigh numbers (Ra) with Pr = 6.2, Rb = 2.0, Da = 0.01, Ha = 2, Le = 2, Pe = 1 $\chi = 1, \sigma_1 = 1$.

In the computations we prescribe values of the controlling parameters as follows: bioconvective Rayleigh number (Rb = 0–100), Peclet number (Pe = 0.1–5.0), Lewis number (Le = 0.1–5.0), porous substance permeability (Da = 10^{-4}–10^{-1}), magnetizing field strength (Ha = 0–25), and Rayleigh number (Ra = 10–10^4). This data is consistent with actual bioconvective magnetic fuel designs [16-20].

Figure 3 illustrates the numerical results for flow patterns (streamlines) and temperature contours with increment in Darcy number (Da). We first consider the streamline plots (left column) and then the isotherm contours (right column). At very low Darcy number i.e. Da = 0.0001 (very small permeability), there are two distinct vortex cells visible in the regime (left column), a larger one towards the left inclined wall and a narrow constricted one towards the right hot vertical wall. Clearly the internal circulation is supressed with low permeability since the Darcian drag force components, -(Pr/Da)ω in the vorticity-stream function reduced momentum eqn. (10) are both enhanced considerably. The lower permeability indicates a reduction in pore space and proliferation in solid material fibers in the porous medium. This produces significant retardation to the circulating magnetic fluid. There is clearly an inverse relationship between Darcian drag force and Darcy number. The bulk matrix resistance to the percolating magnetic fluid is amplified with low permeability. As Darcy number is elevated by a factor of ten to Da = 0.001, permeability is enhanced, since $\mathrm{Da} = \frac{\mathrm{K}}{\mathrm{H}^2}$ i.e. Darcy number is directly proportional to medium permeability (hydraulic conductivity). This causes the dual vortex cell structures to merge into a single larger vortex cell which is orientated diagonally in alignment with the cold left slanted wall of the fuel cell enclosure. While the intensity of circulation remains strongest (red streamline contours, ψ) at the centre of this vortex cell, the vortex cell is stretched increasingly from the top left enclosure corner towards the base horizontal wall. This effect is further exacerbated with a subsequent increase in Darcy number to the maximum value of Da = 0.01. In all cases low velocity blue zones dominate near the hot vertical wall and in the periphery of the vortex cell (boundaries). The internal flow distribution is clearly strongly influenced with a change in porous medium permeability. Regarding the isotherm contours (θ, right column) we observe that high magnitudes consistently arise near the hot vertical wall (right hand side boundary of the enclosure). Isotherms are initially parallel to the vertical hot wall; however, they become increasingly distorted as we progress to the left cold slanted wall and also decrease significantly in magnitude. Strong blue cool zones dominate the left half space of the enclosure. As Darcy number increases, hotter fluid spreads to occupy the upper half space increasingly whereas cooler zones penetrate the lower half space and increasingly impinge on the lower horizontal wall. As Darcy number is increased, the percentage concentration of solid matrix fibers is reduced in the enclosure. This assists percolation of the magnetic fluid but alters heat transfer behaviour. Thermal conduction is reduced due to the depletion of solid material. This results in significant cooling in the lower half space. Internal heat distribution is considerably modified with larger permeability (Darcy number); however, the transport of heat is sustained in the upper right corner of the enclosure although the heated zone is contracted in the lower zone near the horizontal base wall. Sigmoidal patterns are intensified with increasing Darcy number in particular towards the left slanted wall. The permeability of the porous medium clearly exerts a substantial influence on energy transmission in the fuel cell geometry.

Figure 4 depicts the Oxygen iso-concentration (ϕ) and micro-organism density contours (N) with increment in Darcy number (Da). Significantly different topologies are computed for these quantities compared with the streamlines and isotherms. Considering first the oxygen concentration contours, at minimal Darcy number (Da= 0.0001), we observe that a single concentration cell emerges from the upper horizontal adiabatic wall initially and spreads downwards into the enclosure with high oxygen concentrations near the periphery i.e. maximum oxygen concentration arises near the left sloped wall, base adiabatic wall and right hot vertical wall. Evidently as Da is increased to 0.001, the higher initial oxygen concentration at the upper boundary is replaced by lower concentrations. The concentration cell becomes increasingly distorted and higher oxygen diffusion is pushed towards the lower half space with oxygen depletion (blue zone) occupying the upper half space. Increasing permeability i.e. lower concentration of solid fibers therefore assists oxygen transport to the lower half of the fuel cell; however, it curtails oxygen diffusion in the upper half space. However, this trend is altered with subsequent increase in Darcy number to a maximum value of Da = 0.01. The blue low concentration zone of oxygen concentration now contracts considerably, and oxygen diffusion is encouraged to the majority of the fuel cell. Iso-concentration contours become increasingly distorted. However, oxygen distribution is strongly elevated. A critical Darcy number threshold therefore exists beyond which oxygen transport is significantly boosted in the fuel cell and this will in turn elevate efficiency in magnetic microbial fuel cell designs. While Darcy number does not arise explicitly in the oxygen concentration eqn. (12), there is very strong coupling between the momentum eqn. (10) -in which Darcy number features- and the oxygen eqn. (12) via the nonlinear convective diffusion terms, $+U\frac{\partial\phi}{\partial X}$ and $+V\frac{\partial\phi}{\partial Y}$. The influence of Darcy number is therefore imparted indirectly to the oxygen diffusion field. Evidently highly permeable fuel cell materials will encourage the effectiveness of oxygen transport whereas very low permeabilities will inhibit transport. Now inspecting the micro-organism density (iso-concentration) contours (N), we observe that at very low Darcy number (Da = 0.0001) much of the enclosure is occupied by a large blue low magnitude zone indicating weak bacterial (micro-organism) concentrations in the core of the fuel cell. In the peripheral zones higher magnitudes of N are computed. As with the oxygen species eqn. (12), there is no presence of Darcy number in the micro-organism concentration eqn. (13). However once again there is very strong coupling to the momentum eqn. (10) via the micro-organism (bacterial) eqn. (13) nonlinear convective mass diffusion terms, $\chi\left[U\frac{\partial N}{\partial x}+V\frac{\partial N}{\partial y}\right]$. Furthermore, the oxygen and micro-organism equation (13) is coupled via the term, $-\frac{\sigma_1}{Le}N$ in eqn. (12) and the diffusion terms, $-\frac{Pe}{Le}\left[N\frac{\partial^2\phi}{\partial x^2}+N\frac{\partial^2\phi}{\partial y^2}+\frac{\partial N}{\partial x}\frac{\partial\phi}{\partial x}+\frac{\partial N}{\partial y}\frac{\partial\phi}{\partial y}\right]$. In the plots in Fig. 4 only the impact of Darcy number is assessed. We have prescribed strong thermal buoyancy ($Ra = 10^5$), unity oxygen diffusion ratio (χ =1), ratio of oxygen consumption to oxygen diffusion as unity ($\sigma_1 = 1$), bioconvection Rayleigh number Rb = 2 (indicating that micro-organism species buoyancy is dominant), Lewis number Le = 2 (i.e. the thermal diffusivity is double the oxygen molecular diffusivity), bioconvection Péclet number Pe = 1 (i.e. the momentum diffusivity of the swimming micro-organisms and molecular diffusivity are equal). Additionally, Ha =2 i.e. the Lorentz magnetic drag is twice the viscous hydrodynamic force in the enclosure. Clearly the low permeability (Da = 0.0001) results in a strong damping in motile micro-organism concentrations. As Da is increased to 0.001 this blue low magnitude zone which originates at the upper boundary is progressively depleted and micro-organism diffusion is encouraged leading to an expansion of green, yellow, orange, red and brown zones. Peak concentrations in micro-organisms are expanded along the slanted cold wall and also at the hot vertical wall and along the lower boundary. The micro-organism iso-concentrations are also increasingly warped towards the core zone of the enclosure. With maximum Darcy number (Da = 0.01), the low magnitude blue zone at the upper wall is further contracted and higher micro-organism concentrations encroach deeper into the core. Larger permeability values, therefore, as with oxygen concentrations, strongly assists in the promotion of micro-organism self-propulsion in the fuel cell. This is certainly beneficial to magnetic biofuel cell design and confirms the key role of a porous medium in manipulating bacterial concentration distributions as noted by Kim and Fogler [16]. It is also important to note that the thermal buoyancy effect can influence the bacterial motions especially when micro-organism and fluid densities exhibit large differences. Oxytactic micro-organisms may either sink or float which in turn influences their stability and results in hydrodynamic disturbances in the magnetic carrier fluid in the fuel cell [36]. Buoyancy effects are also known to induce velocity modifications in enclosure fuel cell dynamics [17]. There is overall a very delicate interplay between the fluid, thermal, oxygen and micro-organism behaviour all of which are sensitive to multiple effects including the permeability of the porous medium, as simulated by Darcy number. An augmentation in bioconvection Péclet number number (Pe) can also suppress motile micro-organisms concentration [25] owing to biconvection plumes arising and to avoid this we have set this parameter as unity in the computations.

Fig. 5 visualizes the streamline (ψ) and isotherm (θ) contour plots with variation in Rayleigh number (Ra). As Rayleigh number is enhanced from 10^3 to 10^4 and finally 10^5, there is a strong modification in the single vortex cell structure. This cell is attached to the left slanted wall and is progressively expanded laterally towards the hot vertical wall as Rayleigh number is elevated. Thermal buoyancy therefore encourages circulation in the enclosure fuel cell and also expands the higher velocity core zone deeper towards the right hot wall. The elliptic core vortex warps significantly at peak Rayleigh number ($Ra = 10^5$) and becomes deeper towards the left slanted cold wall and narrower towards the right hot wall. The low velocity zone external to the single vortex cell is contracted with greater thermal buoyancy i.e. the blue zone is decreased in magnitude. Streamline magnitudes are higher with greater thermal buoyancy and the fuel cell enclosure is more fully occupied by the vortex cell. The implication is that a modification in thermal buoyancy force, as simulated via the term, $\mathrm{RaPr}\left[\frac{\partial\theta}{\partial X} - \mathrm{Rb}\frac{\partial N}{\partial X}\right]$ in the momentum eqn. (10), generates a significant alteration in internal circulation within the fuel cell. Inspection of the isotherm plots (right column) shows that at all Rayleigh numbers, peak temperatures are computed at and in the vicinity of the right hot wall of the enclosure. Isotherms are largely vertical for low thermal buoyancy effect ($Ra = 10^3$) and only become distorted after some distance into the enclosure from the right wall. This distortion arises more prominently when Ra increases to 10^4 and extends for a much greater proportion of the fuel cell enclosure. However sigmoidal warping in isotherms does not impinge on the vertical wall or immediately adjacent to it. At maximum Rayleigh number, very significant distortion in isotherms is produced and commences near the upper right corner and encroaches throughout the cavity. The cold left blue zone near the inclined wall is progressively depleted and hot fluid penetrates further along the upper boundary and deeper into the core of the enclosure. However, a greater proportion of the lower horizontal adiabatic wall is exposed to this cool zone with maximum Rayleigh number ($Ra = 10^5$). Careful manipulation of thermal buoyancy (as with permeability of the porous medium), can therefore be utilized to successfully manipulate the heat distribution within the magnetic bioconvection fuel cell which holds promise for future designs [22].

Fig. 6 visualizes the Oxygen iso-concentration (ϕ) and micro-organism density contours (N) with increment in Rayleigh number (Ra). Again, there is a very different structure to the plots compared with streamlines and isotherms. As Rayleigh number is enhanced from 10^3 to 10^4 and finally 10^5, there is a strong adjustment in the oxygen iso-concentration distributions. At low Rayleigh number ($Ra = 10^3$) it is evident that a large blue low oxygen concentration semi-circular cell arises and penetrates quite deeply into the fuel cell enclosure. This central cell is surrounded by progressively higher oxygen concentrations towards the other three boundaries (left inclined wall, base adiabatic wall and right vertical hot wall). As Rayleigh number is increased, the iso-concentrations are substantially warped, and the blue low oxygen concentration upper cell expands laterally but contracts vertically. Overall, the lower magnitude zone is reduced in size. Higher oxygen concentrations (green and yellow contours) impeach deeper into the core. With maximum Rayleigh number, ($Ra = 10^5$) the blue zone is further depleted and becomes isolated to a small section in the vicinity of the upper adiabatic horizontal boundary. Oxygen diffusion is strongly encouraged in the enclosure and much higher concentrations are distributed over a greater proportion of the enclosure, dominating the core zone and in particular the lower right corner of the fuel cell. Strong thermal buoyancy (high Rayleigh number) effectively encourages oxygen diffusion throughout the enclosure and produces a much more homogenous distribution relative to weak thermal buoyancy (low Rayleigh number). With regard to the micro-organism density (iso-concentration) contours (N), as visualized in the right column, it is apparent that at low Rayleigh number ($Ra = 10^3$) a much larger low concentration cell is computed which penetrates deep into the fuel cell enclosure, emanating from the upper horizontal boundary. This low concentration semi-elliptic (blue) zone for micro-organisms is much larger than the corresponding oxygen concentration zone. The presence of low concentration micro-organism and also low oxygen iso-concentration zones at the upper boundary is intimately connected to the boundary conditions prescribed there in eqn. (14), viz, $\phi = 1, \mathrm{PeN}\frac{\partial \phi}{\partial Y} - \frac{\partial N}{\partial Y} = 0, \mathrm{at} Y = 0$ (at the lower adiabatic wall) and $\frac{\partial \phi}{\partial Y} = 0, \frac{\partial N}{\partial Y} = 0, \mathrm{at} Y = 1$ (at the upper boundary). For the scenario where the upper layer of the fluid is very thick (near the adiabatic boundary), microorganisms descend, resulting in bioconvection patterns. Certain oxytactic bacteria, like Bacillus subtilis, are known to be propelled by the oxygen they consume as they are oxytactic. Via surface diffusion, however, the oxygen is replenished in natural environmental situations (free surface flows, lakes, oceans etc). However, in fuel cell enclosures as considered here, the oxygen replenishment can be mobilized artificially [17]. As Rayleigh number is increased to 10^4 the blue zone is distorted and contracts diagonally but expands along the upper boundary. The high micro-organism concentration zone along the lower section of the inclined left cold wall is expanded and higher iso-concentrations also emerge at the lower horizontal adiabatic boundary. These trends are further amplified with further increment in Rayleigh number to 10^5, and the blue low micro-organism concentration zone is isolated towards the upper left corner of the enclosure. Higher concentration of micro-organisms is produced in the majority of the enclosure. Thermal buoyancy is therefore observed to strongly accentuate the self-propulsion of micro-organisms (bacteria) in the fuel cell.

Figs. 7 to 9 show the distributions along the right hot vertical wall of local Nusselt number ($\mathrm{Nu} = -\left(\frac{\partial \theta}{\partial Y}\right)_{\mathrm{at}X=2}$) and oxygen concentration Sherwood number ($\mathrm{Sh} = -\left(\frac{\partial \phi}{\partial Y}\right)_{\mathrm{at}X=2}$)) with various selected parameters. Inspection of **Fig. 7** (top plot) reveals that as we progress from the base of the vertical wall (Y =0) to the top (Y = 1), Nusselt number is significantly suppressed i.e. heat transfer rate to the vertical wall is diminished. However, with increasing Darcy number since greater permeability induces a cooling effect within the enclosure, as computed earlier in the contour plots for isotherms, the net effect of larger Darcy number (higher permeability) is a boost in heat diffusing to the vertical wall. This induces a heating effect at the wall boundary and associated elevation in Nusselt number. Maximum Nusselt number for which thermal convection is maximum relative to thermal conduction at the vertical wall, is always computed at the base of the wall and minimal Nusselt number generally arises at the top of the wall. A very different response in oxygen species Sherwood number (lower plot) is observed with increasing Darcy number and also with location along the vertical hot wall of the enclosure. Peak oxygen Sherwood number is computed always at the top of the wall (Y = 1) and the minimal Sherwood number arises at the base (Y = 0).

Sherwood number is observed also to be strongly suppressed with increasing Darcy number. As elaborated earlier, since the oxygen diffusion is encouraged by larger permeability, concentrations are higher within the fuel cell enclosure (bulk flow). This leads to a depletion in oxygen diffusing to the boundary (vertical wall) which manifests in a plummet in oxygen Sherwood number. Clearly therefore both the oxygen diffusion to the internal circulating flow and oxygen migration to the boundaries of the fuel cell (oxygen Sherwood number) can be manipulated effectively with different permeability of the porous medium utilized in fuel cell design. In other words, lower permeability (Darcy number) accentuates the oxygen diffusion rate to the hot vertical wall whereas higher permeability (Darcy number) induces the opposite effect. **Fig. 8** (top plot) shows reveals that as we progress from the base of the vertical wall (Y =0) to the top (Y = 1), Nusselt number is markedly reduced i.e. heat transfer rate to the vertical wall is suppressed and thermal convection becomes dominated increasingly by thermal conduction. With elevation in Hartmann number (Ha) from 0 (non-magnetic case) through 5, 10 to 25, there is a considerable suppression in Nusselt number. The Hartmann number features in the linear Lorentzian magnetic drag term, in the momentum eqn. (10), viz, $-Ha^2 Pr \frac{\partial V}{\partial X}$. As magnetic field is elevated the Lorentzian force is amplified and the magnetic enclosure fluid has to expend more work to drag itself against the action of the increasing electromagnetic impedance force. This supplementary work is dissipated as thermal energy which leads to a boost in isotherm magnitudes (not plotted). As result since heating is induced within the enclosure, the net effect is to draw thermal energy away from the boundaries. Consequently, the Nusselt number at the hot vertical wall is depleted as observed in Fig. 8. In practical magnetic fuel cell operations, this reduction in heat transfer at the boundary is advantageous since it permits thermal management to be achieved and mitigates over-heating of the fuel cell boundaries which could lead to corrosion and other operational problems [19]. Inevitably the oxygen levels in the fuel cell will also contribute to corrosion, although this aspect has not been considered in the current simulations and may be addressed in future investigations. Generally magnetic field is found to be very beneficial for heat control at the vertical wall and simultaneously elevates temperatures within the enclosure fuel cell leading to enhanced thermal fuel cell efficiencies. While Fig 8 (lower) also demonstrates that oxygen Sherwood number is reduced with magnetic field (Hartmann number); however, the topology of the profiles is very different as we progress from the base to the top of the hot vertical wall. Oxygen Sherwood number profiles oscillate with distance along the wall. The peak value arises a greater distance above the base of the wall and while magnitudes plummet at the top of the wall, they are considerably greater than for the Nusselt number. A relatively high oxygen Sherwood number is therefore sustained along the vertical wall whereas Nusselt number is only high near the base of the wall, at any value of Hartmann number. Finally, **Fig. 9** shows the impact of Rayleigh number (Ra) on local Nusselt number (top plot) and oxygen species Sherwood number (lower plot) along the right vertical hot boundary. As Rayleigh number increases, Nusselt number is strongly boosted at the base of the wall (Y =0). However further up the wall, beyond the mid-point (Y =0.5), this trend is reversed and Nusselt number is suppressed with greater Rayleigh number. For the minimal Rayleigh number ($Ra = 10^3$), the Nusselt number essentially remains invariant along the entire extent of the vertical wall. However, for higher Rayleigh numbers heat transfer rate to the vertical wall is boosted in the lower half-section ($0< Y<0.5$) but depleted in the upper half section ($0.5< Y< 1$). Thermal buoyancy therefore has a complex influence on heat transfer rate to the vertical boundary. This behaviour is spatially dependent and associated with the location along the vertical wall. A more consistent response is computed for the oxygen Sherwood number. Magnitudes are consistently decreased with increasing Rayleigh number since oxygen diffusion within the enclosure fuel cell is encouraged with greater thermal buoyancy, as observed in earlier contour plots. Effectively therefore thermal buoyancy opposes the diffusion of oxygen in the fuel cell from the interior to the boundary and this produces the depletion in oxygen Sherwood numbers. Peak oxygen Sherwood number is always observed at the top of the vertical wall and the minimum value corresponds to the base of the wall. In magnetic biofuel cell design, therefore it is apparent that oxygen transport can be boosted or suppressed depending on the intensity of natural thermal convection (buoyancy) within the regime. This can be exploited by fuel cell designers to achieve optimal rates of oxygen mass transfer to or from specific boundaries.

5. CONCLUSIONS

As a simulation of a hybrid magnetohydrodynamic (MHD) biconvection fuel cell, a mathematical model has been developed to study theoretically and numerically thermal/species/momentum characteristics in two-dimensional triple convection flow in a semi-trapezoidal enclosure saturated with electro-conductive water containing oxytactic micro-organisms and oxygen species. Darcy's model has been deployed to simulate porous media drag effects. The transport equations for mass, momentum, energy, oxygen species and motile micro-organism species density have been transformed into non-dimensional form using a vorticity-stream function formulation and appropriate dimensionless variables. The model has been shown to be controlled by several key dimensionless numbers, namely, parameters i.e. Prandtl number, Rayleigh number, Bioconvective Rayleigh number, Darcy parameter, Hartmann (magnetic body force) number, Lewis number, Péclet number, Oxygen diffusion ratio and fraction of consumption oxygen to diffusion of oxygen parameter. This nonlinear boundary value problem has been solved computationally with a well-tested finite difference method with incremental time steps is deployed to obtain computational solutions. Validation with previous studies has been included. The transport characteristics (streamlines, isotherms, species iso-concentration and motile micro-organism concentration) have been studied for the effects of selected parameters. Local Nusselt number and oxygen Sherwood number at the vertical hot wall of the enclosure have also been computed. The main findings of the present analysis may be summarized as follows:

i) With increasing Rayleigh number (Ra), Nusselt number is initially elevated at the base of the right hot vertical wall (Y =0), whereas further up the wall, beyond the mid-point (Y =0.5), this trend is reversed and Nusselt number is suppressed with greater Rayleigh number.

ii) With elevation in Rayleigh number, the oxygen iso-concentrations are greatly distorted, evolving into sigmoidal topologies, and the original (blue contour) low oxygen concentration upper cell is stretched laterally but contracts vertically. Furthermore, greater oxygen concentrations (green and yellow contours) incur more deeply into the fuel cell central region.

iii) With greater Rayleigh number A significantly higher concentration of micro-organisms is produced in the majority of the enclosure. Thermal buoyancy significantly assists the self-propulsion of micro-organisms (bacteria) in the fuel cell.

iv) With increasing Darcy number (Da), oxygen Sherwood number is considerably depleted. Peak oxygen Sherwood number is computed always at the top of the wall (Y = 1) and the minimal Sherwood number arises at the base (Y = 0).

v) With increasing Darcy number (Da), peak concentrations in micro-organisms are expanded along the slanted cold wall and also at the hot vertical wall and along the lower boundary. Larger permeability values, therefore, as with oxygen concentrations, strongly assist in the promotion of micro-organism self-propulsion in the fuel cell, producing higher performance efficiencies.

vi) With increasing Hartmann number (Ha) i.e. stronger magnetic field, oxygen Sherwood number is significantly reduced at the right hot vertical wall, and similarly there is a strong reduction in local Nusselt number.

The current study has revealed some novel features of oxygen diffusion and oxytactic micro-organism (bacterial) dynamics in hybrid magnetic porous media fuel cells. Future investigations may consider in more detail the effects of oxygen consumption and also non-Newtonian working fluid effects which are also of interest in 21st century fuel cell technologies. Additionally, wavy boundary geometries and nanofluids [37-40] may be considered.

NOMENCLATURE:

Roman

B_0 Magnetic field strength $\left[kg\, s^{-2} A^{-1}\right]$

C Dimensional oxygen concentration $\left[kg\, m^{-3}\right]$

C_c Low concentration $\left[kg\, m^{-3}\right]$

C_h High concentration $\left[kg\, m^{-3}\right]$

D_c Oxygen diffusivity $\left[m^2 s^{-1}\right]$

D_n Bacteria' diffusivity $\left[m^2 s^{-1}\right]$

Da Darcy number $[-]$

g Acceleration due to gravity $\left[m\, s^{-2}\right]$

Gr Grashof number $[-]$

H Height of the enclosure $[m]$

Ha Hartmann number $[-]$

K Permeability of the porous medium $\left[m^2\right]$

L Length of the cavity $[m]$

Le Lewis number

n Density of motile microorganisms $\left[kg\, m^{-3}\right]$

Nu Local Nusselt number $[-]$

p Dimensional pressure [Pa]

P Dimensionless pressure $[-]$

Pr Prandtl number $[-]$

Ra Rayleigh number $[-]$

Rb Bioconvective Rayleigh number

t Dimensional time $[s]$

T Dimensional temperature of the fluid $[K]$

T_h Temperature of the hot wall $[K]$

T_c Temperature of the cold wall $[K]$

U,V Dimensionless velocities along X and Y directions $[-]$

u,v Dimensional velocity components in x and y directions $[m\,s^{-1}]$

U_0 Constant reference velocity $[m\,s^{-1}]$

X,Y Dimensionless Cartesian coordinates $[-]$

$x;y$ Dimensional Cartesian coordinates $[m]$

Greek

β Thermal expansion coefficient $[K^{-1}]$

δn Consumption of microorganisms

ϕ Dimensionless concentration $[-]$

θ Dimensionless temperature $[-]$

σ Electrical conductivity of the fluid $[S\,m^{-1}]$

μ Dynamic viscosity of the fluid $[kg\,m^{-2}s^{-1}]$

ν Kinematic viscosity of the fluid $[m^{-2}s^{-1}]$

α Thermal diffusivity of the fluid $[m^{-2}s^{-1}]$

ρ_f Density of the fluid $[kg\,m^{-3}]$

ρ_p Density of the nanoparticle $[kg\,m^{-3}]$

REFERENCES

[1] P. Geng, A.V. Kuznetsov, Effect of small solid particles on the development of bioconvection plumes, *Int. Commun. Heat Mass Transfer,* 31 (2004) 629–638.

[2] A.V. Kuznetsov, New developments in bioconvection in porous media: bioconvection plumes, bio-thermal convection, and effects of vertical vibration, In *P. Vadasz (ed.), Emerging Topics in Heat and Mass Transfer in Porous Media*, Springer Science+Business Media B.V. (2008).

[3] J.O. Kessler, The external dynamics of swimming micro-organisms, *Progr. Phycol. Res*. 4 (1986) 258–307

[4] Stephenson AL, Kazamia E, Dennis JS, Howe CJ, Scott SA, Smith AG. Life-cycle assessment of potential algal biodiesel production in the United Kingdom: a comparison of raceways and air-lift tubular bioreactors. *Energy Fuels* 24, 4062–4077 (2010).

[5] Scott SA, Davey MP, Dennis JS et al. Biodiesel from algae: challenges and prospects. *Curr. Opin. Biotechnol.* 21(3), 277–286 (2010).

[6] M. Shamshuddin, S.R. Mishra, Ali Kadir and O. Anwar Bég, Unsteady chemo-tribological squeezing flow of magnetized bioconvection lubricants: *numerical study, J. Nanofluids,* 8 (2) 407-419 (2019).

[7] N. Acharya, R. Bag and P.K. Kundu, Unsteady bioconvective squeezing flow with higher-order chemical reaction and second-order slip effects, *Heat Transfer*, 2021.

[8] N. Islam Nima, M. Ferdows, O. Anwar Bég, S. Kuharat and A. Nakayama, Biomathematical model for gyrotactic free-forced bioconvection with oxygen diffusion in near-wall transport within a porous medium fuel cell, *Int. J Biomathematics* (2020). 2050026 (25 pages). DOI: 10.1142/S1793524520500266

[9] J. Zhang et al. (Eds)., *PEM Fuel Cell Electrocatalysts and Catalyst Layers: Fundamentals and Applications*, ed. J. Zhang, Springer Science & Business Media, 2008.

[10] Balan, B., Dhaulaniya, A. S., Varma, D. A., Sodhi, K. K., Kumar, M., Tiwari, M., & Singh, D. K. (2021). Microbial biofilm ecology, in silico study of quorum sensing receptor-ligand interactions and biofilm mediated bioremediation. *Archives of Microbiology*, 203(1), 13e30

[11] Ettwig, K. F., Butler, M. K., Le Paslier, D., Pelletier, E., Mangenot, S., Kuypers, M. M., … Strous, M. (2010). Nitrite-driven anaerobic methane oxidation by oxygenic bacteria. *Nature*, 464(7288), 543e548

[12] Ettwig, K. F., Speth, D. R., Reimann, J., Wu, M. L., Jetten, M. S., & Keltjens, J. T. (2012). Bacterial oxygen production in the dark. *Frontiers in Microbiology,* 3, 273.

[13] Hulsen, T., Hsieh, K., Lu, Y., Tait, S., & Batstone, D. J. (2018). Simultaneous treatment and single cell protein production from agri-industrial wastewaters using purple phototrophic bacteria or microalgaeea comparison. *Bioresource Technology*, 254, 214e223

[14] Islam, M. S., Akter, R., Rahman, M. M., & Kurasaki, M. (2022). Phytoremediation: Background, principle, and application, plant species used for phytoremediation. In *S. Tanaka et al. (Eds), Design of Materials and Technologies for Environmental Remediation, Sringer, Germany* (2022).

[15] H. Yuan *et al.* Oxygen reduction reaction catalysts used in microbial fuel cells for energy-efficient wastewater treatment: a review, *Mater. Horiz.*, 2016, 3, 382-401.

[16] Kim D-S, Fogler HS (2000) Biomass evolution in porous media and its effects on permeability under starvation conditions. *Biotechnology and Bioengineering* 69: 47–56.

[17] F.J. Chi *et al.,* Effects of magnetic fields on electricity generation in a photosynthetic ceramic microbial fuel cell, *International Journal of Hydrogen Energy*, 46, 11411-11418 (2021).

[18] E. Katz *et al.,* Magnetic field effects on bioelectrocatalytic reactions of surface-confined enzyme systems: enhanced performance of biofuel cells**,** *J. Amer. Chem Soc*., 2005 Mar 23;127(11):3979-88.

[19] Tatsuhiro Okada *et al.*, The effect of magnetic field on the oxygen reduction reaction and its application in polymer electrolyte fuel cells, *Electrochimica Acta*, 48, 531-539 (2003).

20] H. Zhou *et al.,* Magnet anode enhances extracellular electron transfer and enrichment of exo-electrogenic bacteria in bio-electrochemical systems**,** *Biotechnology for Biofuels*, 12, Article number: 133 (2019).

21] Li WW, Sheng GP, Liu XW, Cai PJ, Sun M, Xiao X, et al. Impact of a static magnetic field on the electricity production of *Shewanella*-inoculated microbial fuel cells. *Biosens Bioelectron*. 26:3987–92, 2011.

22] Tong ZH, Yu HQ, Li WW, Wang YK, Sun M, Liu XW, *et al*. Application of a weak magnetic field to improve microbial fuel cell performance. *Ecotoxicology*. 24: 2175–80, 2015.

23] Yin Y, Huang G, Tong Y, Liu Y, Zhang L. Electricity production and electrochemical impedance modeling of microbial fuel cells under static magnetic field. J Power Sources. 237:58–63, 2013.

24] Sakai Y, Nitta Y, Takahashi F. A submerged filter system consisting of magnetic tubular support media covered with a biofilm fixed by magnetic force. *Water Res*. 28: 1175–9 (1994).

25] M. Taheri, E. Bilgen, Bioconvection of gravitactic micro-organisms in rectangular enclosures, *International Journal of Heat and Mass Transfer*, 50, 4652-4660 (2007).

26] S. Hussain *et al.*, Bioconvection of oxytactic microorganisms with nano-encapsulated phase change materials in an omega-shaped porous enclosure, *Journal of Energy Storage*, 56, 105872 (2022).

27] C. S. Balla *et al.*, Bioconvection in oxytactic microorganism-saturated porous square enclosure with thermal radiation impact, *Journal of Thermal Analysis and Calorimetry,* 140: 2387–2395, 2020.

28] K. Venkatadri, O. Anwar Bég, P. Rajarajeswari, V. Ramachandra Prasad, A. Subbarao and B. Md. Hidayathulla Khan, Numerical simulation and energy flux vector visualization of radiative-convection heat transfer in a porous triangular enclosure, *J. Porous Media, 23(12):1–13 (2020) (13 pages).*

29] O. Anwar Bég, K. Venkatadri, V.R. Prasad, Tasveer A. Bég, Henry J. Leonard, MAC computation of magnetohydrodynamic convection flow in a non-Darcian porous enclosure saturated with electrically conducting Helium, *Proc. IMechE-Part C – J. Mechanical Engineering Science (2021). 21 pages. DOI: 10.1177/09544062211003624*

[30] S. Hussain and B. P. Geridonmez, Mixed bioconvection flow of Ag-MgO/water in the presence of oxytactic bacteria and inclined periodic magnetic field, *International Communications in Heat and Mass Transfer* 134, 106015, 2022.

[31] K. Venkatadri, K. V. N. Murthy, T. A. Bég, O. Anwar Bég, S. Kuharat, Numerical simulation of natural convection in a rectangular enclosure filled with porous medium saturated with magnetic nanofluid using Buongiorno's two-component model, *Can. J. Chem. Eng*. 2024, 1. https://doi.org/10.1002/cjce.25300

[32] K. Venkatadri, O. Anwar Beg, P Rajarajeswari, V. Ramachandra Prasad, Numerical simulation of thermal radiation influence on natural convection in a trapezoidal enclosure: heat flow visualization through energy flux vectors, *International Journal of Mechanical Sciences*, 171 (2020) 105391.

[33] Venkatadri, K., Bég, O.Anwar & Kuharat, S. Magneto-convective flow through a porous enclosure with Hall current and thermal radiation effects: numerical study. *Eur. Phys. J. Spec. Top*. (2022). https://doi.org/10.1140/epjs/s11734-022-00592-9

[34] Bég, O. Anwar, Venkatadri, K., Prasad, V. R., Beg, T. A., Kadir, A., & Leonard, H. J., Numerical simulation of hydromagnetic Marangoni convection flow in a Darcian porous semiconductor melt enclosure with buoyancy and heat generation effects, *Materials Science and Engineering: B*, 261 (2020) 114722. https://doi.org/10.1016/j.mseb.2020.114722

[35] Venkatadri, K., Fazuruddin, S., Anwar Bég, O., & Ramesh, O. (2023). Natural convection of nanofluid flow in a porous medium in a right-angle trapezoidal enclosure: a Tiwari and Das' nanofluid model. *Journal of Taibah University for Science***,** 17 (1). https://doi.org/10.1080/16583655.2023.2263224

[36] Lee, S. Y., and Kim, H. U., Systems strategies for developing industrial microbial strains, *Nature Biotechnology*, vol. 33, no. 10, pp. 1061-1072, 2015.

[37] M.J. Uddin, W.A. Khan, S.R. Qureshi, O. Anwar Bég, Bioconvection nanofluid slip flow past a wavy surface with applications in nano-biofuel cells, *Chin. J. Phys*. 55 (5) (2017) 2048–2063.

[38] K. Elsaid, M.A. Abdelkareem, H.M. Maghrabie, E.T. Sayed, T. Wilberforce, A. Baroutaji, A.G. Olabi, Thermophysical properties of graphene-based nanofluids, *Int. J. Thermofluids* 10 00073, 2021.

[39] B.M.J. Rana, S.M. Arifuzzaman, S. Islam, S. Reza-E-Rabbi, A. Al-Mamun, M. Mazumder, K.C. Roy, M.S. Khan, Swimming of microbes in blood flow of nano-bioconvective Williamson fluid, *Therm. Sci. Eng. Progr*. 25, 101018, 2021.

[40] A. Kuznetsov, The onset of nanofluid bioconvection in a suspension containing both nanoparticles and gyrotactic microorganisms, *Int. Commun. Heat Mass Transfer* 37 (10) (2010) 1421–1425.